



Surface Integrity of Binderless WC Using Dry Electrical Discharge Assisted Grinding

YanJun Lu¹ · Xingyu Mou¹ · Huapan Xiao² · Kangsen Li² · Chunjin Wang²

Received: 22 December 2023 / Revised: 7 April 2024 / Accepted: 9 April 2024
© The Author(s) 2024

Abstract

Binderless tungsten carbide (WC) is preferred for manufacturing tools, mould, and wear-resistant components. However, due to its high brittleness and hardness, the machined binderless WC surface is prone to generate microcracks and the machining efficiency is extremely low. Aiming at this difficulty, a clean and eco-friendly dry electrical discharge assisted grinding (DEDAG) method without any liquid medium was proposed for the processing of binderless WC. DEDAG principle was revealed and the DEDAG platform was first developed. A series of DEDAG, conventional dry grinding (CDG), and conventional wet grinding (CWG) experiments were conducted on binderless WC under different processing parameters. The current and voltage waveforms during the DEDAG process were observed, and the discharge properties were analyzed. The chip morphologies, surface hardness, residual stress, as well as surface and subsurface morphologies were analyzed. The results show that the surface hardness and roughness obtained by DEDAG are smaller than that by CDG or CWG. The measured residual tensile stress after CDG is larger against DEDAG. The ground surface by DEDAG has better crystal integrity than that by CDG. DEDAG can soften/melt workpiece material and diminish grinding chips, thereby promoting plastic removal and increasing processing efficiency. The influences of DEDAG parameters on the ground surface quality are also investigated, and the optimal DEDAG parameters are determined. With the increase of open-circuit voltage or grinding depth, the surface quality improves first and then worsens. The optimal open-circuit voltage is 40 V and the grinding depth ranges from 10 μm to 15 μm . This research provides a new idea for promoting the efficient and low-damage processing of binderless WC.

Keywords Electrical discharge assisted grinding · Binderless WC · Surface integrity · Surface roughness · Subsurface damage

1 Introduction

As a typical cemented carbide, binderless tungsten carbide (WC) has excellent mechanical and physical properties as well as chemical stability, which is the preferred material for

manufacturing tools, mould, and wear-resistant semiconductor components [1]. For example, binderless WC tool has high toughness, good cutting performance, and long service life, which is suitable for machining hard metal materials, such as titanium alloy [2]. Binderless WC mould has higher hardness and better wear resistance compared with a traditional one with metal binding phases [3]. Moreover, it can avoid the degradation of the mould quality caused by the difference in the thermal diffusion coefficient between metal binding phases and cemented carbide particles [4]. However, during the machining process of binderless WC, it is prone to generate microcracks due to its high brittleness, as well as rupture and fragmentation of WC grains [5], which tremendously reduces the service performance and life [6]. Meanwhile, the tool used for machining binderless WC is easy to wear due to its high hardness, which greatly influences production efficiency. Therefore, how to machine binderless WC with high surface quality and efficiency has always been a research hotspot.

✉ Huapan Xiao
xhp0698@126.com

✉ Chunjin Wang
chunjin.wang@polyu.edu.hk

¹ Guangdong Provincial Key Laboratory of Micro/Nano Optomechatronics Engineering, College of Mechatronics and Control Engineering, Shenzhen University, Shenzhen 518060, China

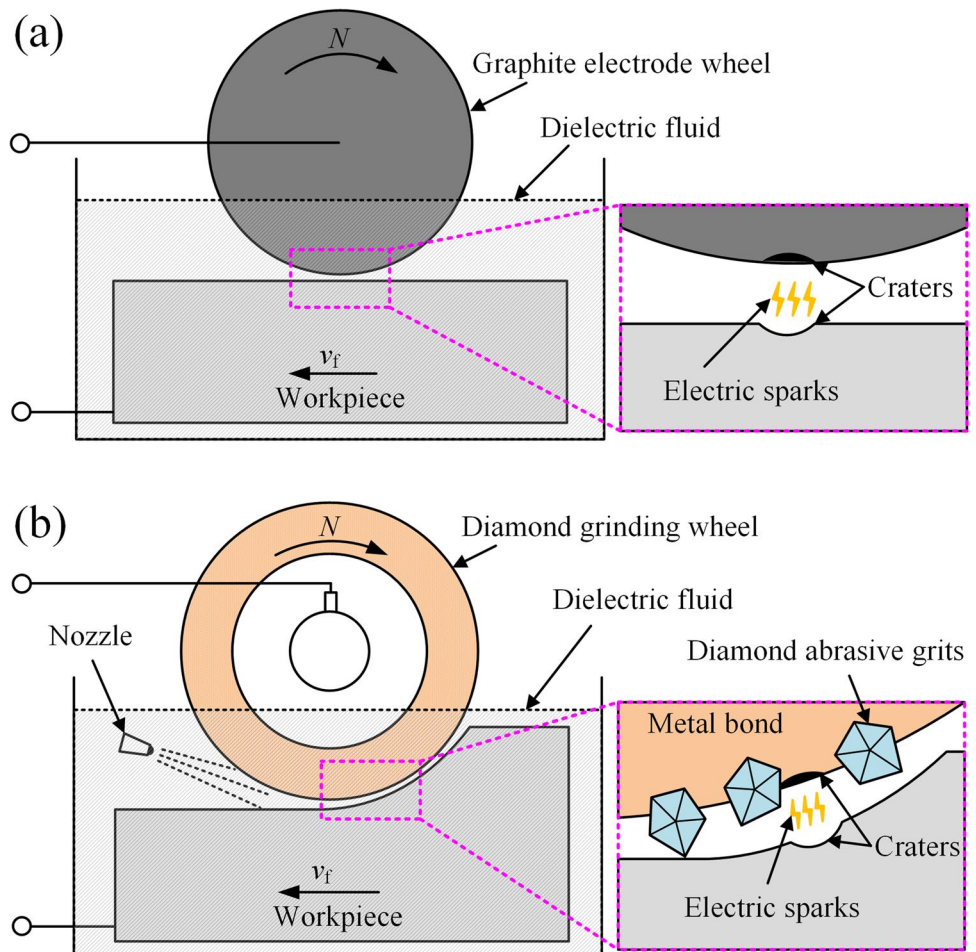
² State Key Laboratory of Ultra-Precision Machining Technology, Department of Industrial and Systems Engineering, The Hong Kong Polytechnic University, Chan Sui Wai Building, Hung Hom, Kowloon, Hong Kong, China

At present, the machining techniques of binderless WC mainly include ultra-precision turning and grinding. The ultra-precision turning can be used to machine the surface with sub-nanometer roughness. For example, Bulla et al. [7] demonstrated that the ductile-mode diamond turning of binderless WC was feasible. You et al. [8] used high effective laser assisted diamond turning to machine binderless WC, and a surface roughness of 0.92 nm (S_a) was achieved. However, some problems still need to be addressed, such as tool wear, chip adhesion, and diamond graphitization, which deteriorate the surface quality. The ultra-precision grinding is often used to process the functional and micro-structured surfaces of binderless WC. It is the most widely used precision machining method in product manufacturing [9]. For example, Zhang et al. [10] adopted single-point diamond grinding with a specialized dressing method to machine the water-drop surface of binderless WC with a form accuracy of 0.64 μm (PV) and a surface roughness of 6 nm (S_a). Guo et al. [11] used up-cut grinding to machine the micro-structured surface of binderless WC, the bottom and side of which had an average surface roughness of 78 nm and 60 nm (S_a), respectively. They also proposed a novel ultrasonic

vibration-assisted grinding method to manufacture a linear microcylinder array with a surface roughness less than 50 nm and an edge radius less than 1 μm [12]. Yan et al. [13] proposed a three-linear-axis ultra-precision grinding with wheel path generation, tool interference checking and profile compensation. And an aspheric mould insert on binderless WC was processed with a mirror surface with surface roughness of less than 8 nm (S_a). Although ultra-precision grinding has a larger material removal rate (MRR) than ultra-precision turning, the high abrasive wear, wheel clogging, and frequent dressing and truing have not been effectively solved, extremely limiting the processing efficiency.

To improve the processing efficiency, some researchers used electrolytic in-process dressing (ELID) grinding to machine cemented carbide. For example, Kim et al. [14] developed an ELID system to realize the mirror-like grinding of WC-Co with a surface roughness of 20 nm (R_a), leading to the decrease in grinding force and reduction in wheel breakage. Stephenson et al. [15] processed the Ni-Cr-B-Si/10vol%WC with a minimum surface roughness of 6 nm (R_a) by ELID grinding. Some researchers also used electrical discharge grinding (EDG) and electrical discharge

Fig. 1 Schematics for (a) electrical discharge grinding (EDG), and (b) electrical discharge diamond grinding (EDDG)



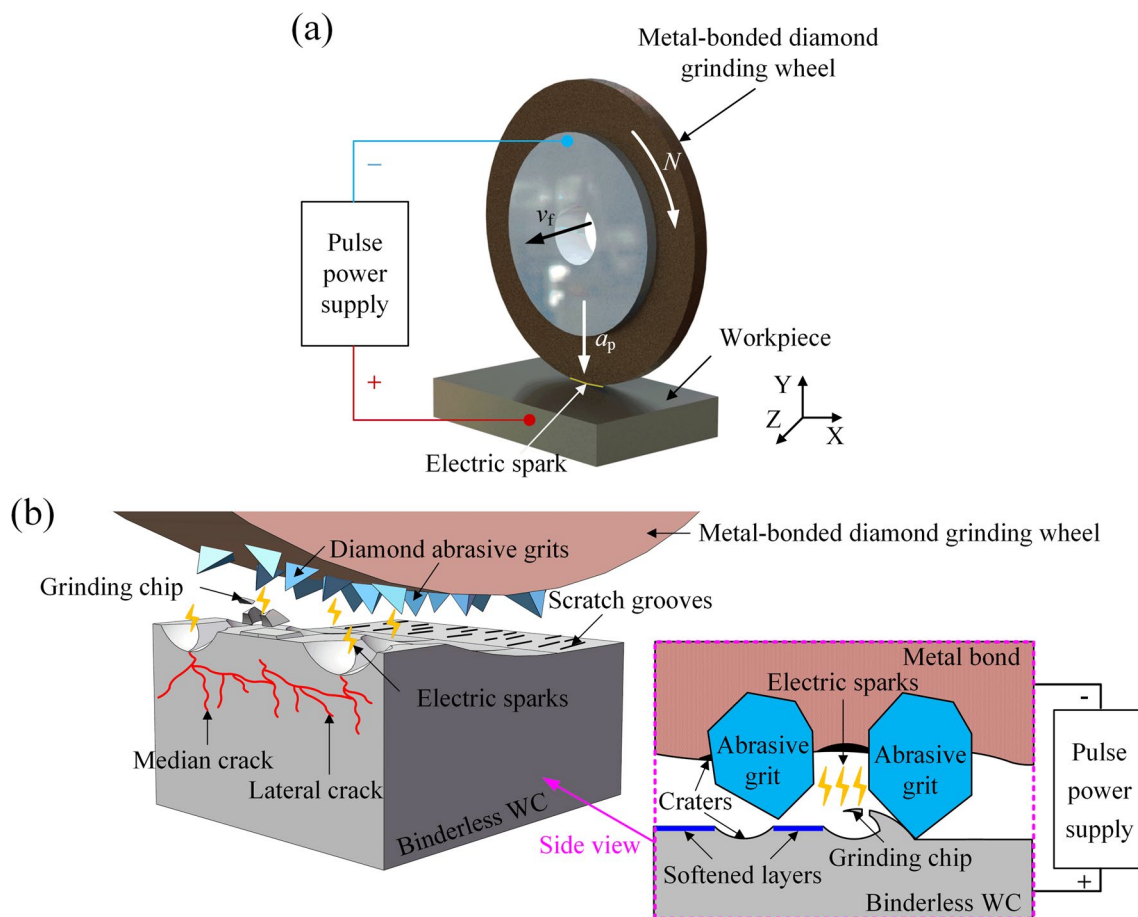


Fig. 2 Schematics of DEDAG (a) platform and (b) principle

diamond grinding (EDDG). As shown in Fig. 1, conventional EDG method utilized the electrode wheel (usually graphite) to process the workpiece. However, the method is often accompanied by post-treatments like polishing and shot peening to remove the heat-affected zone (HAZ) and its attendant defects. To avoid the problem, the EDDG, combining electrical erosion and mechanical removal, was proposed. For example, Koshy et al. [16] investigated the influences of gap current and impulse width on the MRR of WC-TiC-(TaNb)C-Co during EDDG. Singh et al. [17] demonstrated that MRR is positively correlated with current or wheel speed while it is negatively correlated with impulse width during the electro-discharge diamond face grinding (EDDFG) of WC-Co (10wt.% Co). Yadav et al. [18] studied the influences of wheel speed, gap current, impulse width, and duty cycle on MRR during the electrical discharge diamond cutoff grinding (EDDCG) of WC-Co (6wt.% Co).

However, most ELID grinding and EDDG methods use a liquid medium as the dielectric, which is toxic to the human body [19], and can cause resource waste and environmental pollution to a certain extent [20]. Besides, subsurface damages (SSDs) have not been effectively solved during the

machining of cemented carbide [21]. Although there have been reports of using dry electrical discharge for dressing and truing grinding wheels [22, 23], as well as dry wire EDM [24], dry electrical discharge milling [25], and dry micro-EDM [26], it has not been utilized for the surface grinding of binderless WC.

To solve the above problems, comprehensively considering the machining quality, efficiency, and environmental protection, a clean and eco-friendly dry electrical discharge assisted grinding (DEDAG) method is proposed in this paper. The method has rarely been reported previously, and was firstly utilized in the surface grinding of binderless WC. The proposed method can restrain the generation of SSDs since the involve of the electrical discharge promotes the plastic removal of workpiece material. Meanwhile, it can melt and diminish the grinding chips and maintain a certain chip holding space.

In this paper, DEDAG principle is revealed and DEDAG platform is developed. A series of DEDAG, conventional dry grinding (CDG), and conventional wet grinding (CWG) experiments are conducted on binderless WC workpieces under different processing parameters. The current and

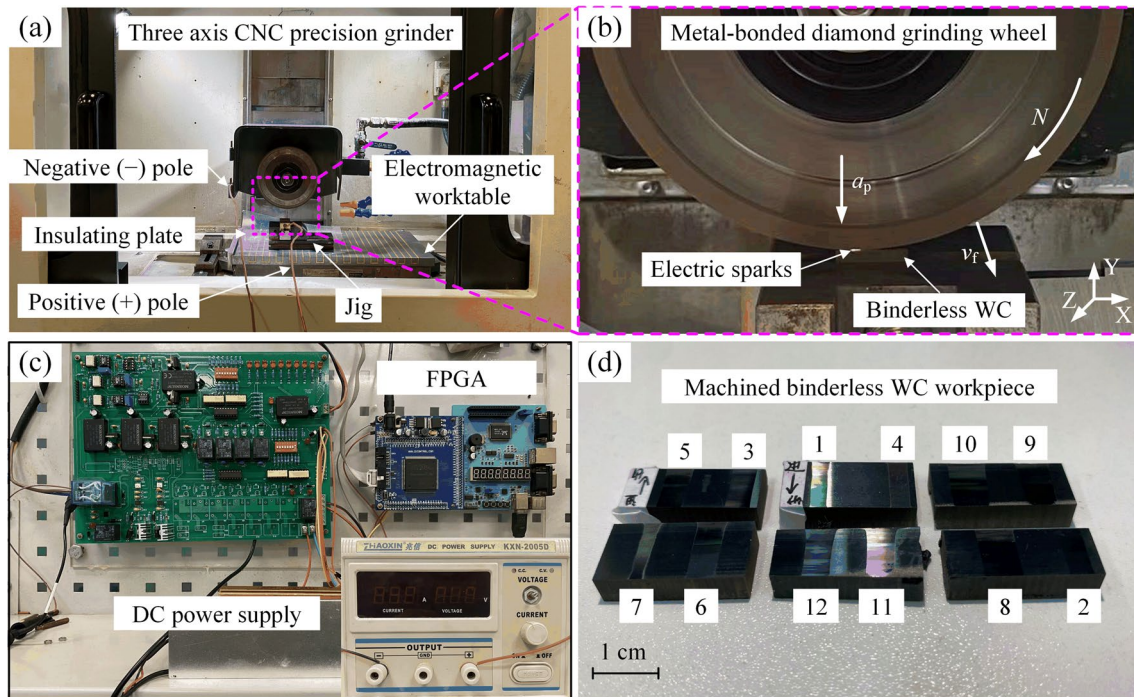


Fig. 3 **a** DEDAG platform for binderless WC; **b** partial enlarged view of (a); **c** direct current (DC) power supply and field programmable gate array (FPGA); and **d** the final machined binderless WC workpieces

Table 1 Specifications parameters of metal-bonded diamond grinding wheel

Type	Bond	Diameter	Thickness	Grain size	Concentration
D150-T5-X10-H31.75	Cu-Sn alloy	Φ150 mm	8 mm	SD400 (38 μm)	100%

Table 2 Material properties of metal-bonded diamond grinding wheel

	Density	Hardness	Specific Heat	Thermal Conductivity	Melting point
Diamond abrasive	2.515 g/mm ³	10,000 Hv	1827 J/kg·K	2000 W/m·K	3700–4000 C°
Metal bond (Cu-Sn)	8.9 g/mm ³	> 620 Hv	384 J/kg·K	105 W/m·K	950 C°

Table 3 Material properties of binderless WC

Density	Hardness	Transverse Rupture Strength	Toughness	Specific Heat	Thermal Conductivity	Thermal Expansion	Electrical Resistivity	Melting point
> 15.4 g/mm ³	> 2700 Hv	> 830 MPa	5.9 MPa/m ²	180.9 J/kg·K	120 W/m·K	4.5 × 10 ⁻⁶ /C°	17 × 10 ⁻⁶ Ω·cm	2870 C°

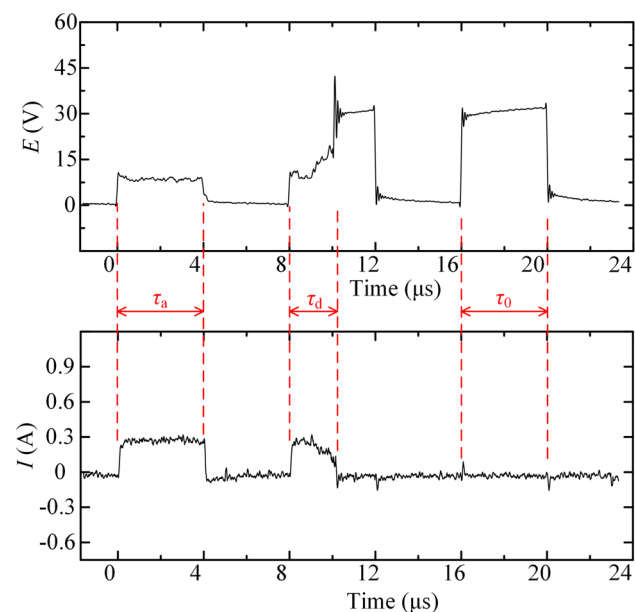
voltage waveforms during the DEDAG process were observed, and the discharge properties were analyzed. The chip morphology, workpiece hardness, residual stress, surface and subsurface morphologies by CDG, DEDAG, and CWG are compared. The effects of open-circuit voltage and grinding depth on the machined surface quality are investigated, and their optimal values are determined.

2 Principle of DEDAG

Figure 2a and b show the schematics of DEDAG platform and principle. Since the discharge energy allocated to the anode is higher than the cathode [27], the grinding wheel and binderless WC workpiece are connected to the negative electrode and positive electrode of high-frequency

Table 4 Processing parameters for CDG, DEDAG, and CWG of binderless WC

Workpiece No	Open-circuit voltage E (V)	Grinding depth a_p (μm)	Grinding coolant
1	0	5	None
2	0	10	None
3	20	5	None
4	30	5	None
5	40	5	None
6	50	5	None
7	30	1	None
8	30	10	None
9	30	15	None
10	30	20	None
11	0	5	6.7 vol% emulsified oil and 93.3 vol% distilled water
12	0	10	6.7 vol% emulsified oil and 93.3 vol% distilled water

**Fig. 4** The current and voltage waveforms during the DEDAG process of binderless WC workpieces

pulse power supply, respectively. The discharge medium is air. DEDAG of binderless WC is feasible since it has good electrical and thermal conductivity. Compared with conventional WC with metal binder (usually Co), there are no metal binding phases in binderless WC. Therefore, the phase-difference-induced erosion sequence and

discharge gap do not change during the machining process. This may reduce the abnormal discharge, and furthermore reduce pits, pores, and cracks [4, 28]. Meanwhile, DEDAG is clean and eco-friendly since it does not need a liquid medium (such as spark oil). As the breakdown strength of air is lower than that of a liquid medium, the discharge gap is very short, easily leading to the generation of electrical discharge [29]. There are three material removal modes including diamond abrasive scratching, electrical discharge erosion, and scratching-erosion combination in DEDAG, which mainly depend on open-circuit voltage and grinding depth [30]. In abrasive scratching, the abrasive grits on grinding wheel surface cut binderless WC resulting in the formation of scratch grooves, grinding chips, median and lateral cracks [31]. In discharge erosion, the electric sparks produce a high temperature of 8000 to 10,000 °C at the discharge center which softens, melts, and vaporizes binderless WC, grinding chips, and metal bond in the grinding wheel. Under the optimal parameters, this causes softened layers and craters on the workpiece surface [32, 33], thereby promoting the plastic removal and suppressing the generation of SSDs. This shrinks the chips and maintains a certain chip holding space, thereby reducing the influences of chip adhesion and scratching on the ground surface. In dry grinding process, thermal load is the main factor contributing to abrasive wear [34]. However, by removing the metal bond, DEDAG can increase the protrusion of abrasive grits, maintain the shape of the abrasive grits and sharpness of the cutting edge, thereby realizing the sharpening of grinding wheel and improving the processing efficiency [35].

3 Experimental

According to DEDAG principal, DEDAG platform was developed for processing binderless WC. As shown in Fig. 3a and b, a three-axis CNC precision grinder (CHEVALIER, SMART-B818III) with a metal-bonded diamond grinding wheel was used to grind a series of binderless WC workpieces. The specifications parameters and material properties of grinding wheel are shown in Tables 1 and 2, respectively. The workpiece size was 10 mm × 20 mm × 5 mm, and its material properties are shown in Table 3. The workpiece was fixed by a jig on the electromagnetic worktable. There was an insulating plate between the jig and the worktable. To produce the high-frequency pulse power, the direct current (DC) power supply and field programmable gate array (FPGA) were used, as shown in Fig. 3c. The grinding wheel performed the axial feeding and reciprocating motion on the workpiece surface, and electric sparks were produced. The size of the discharge gap is critical in controlling the degree

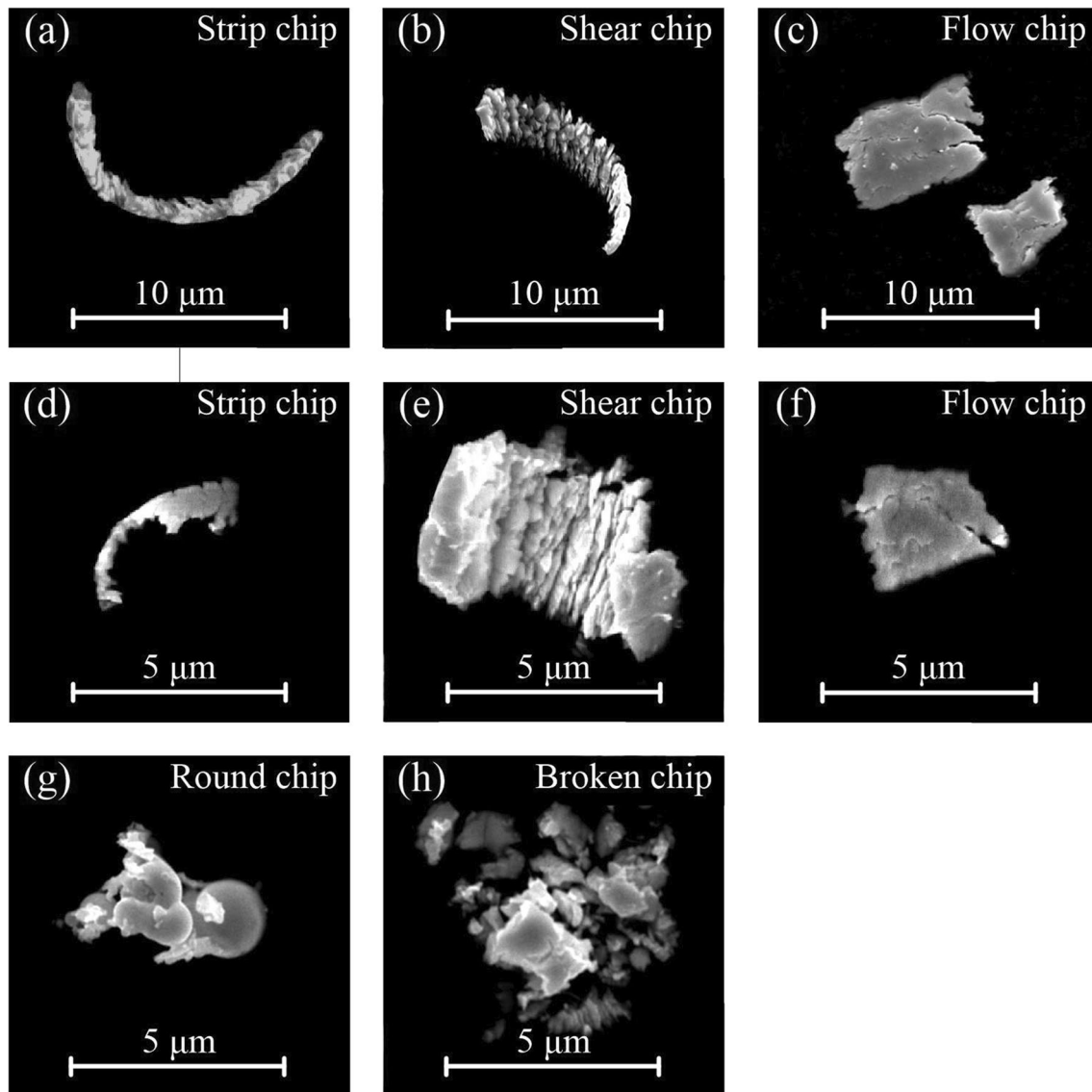


Fig. 5 SEM images of chip morphologies during (a) to (c) CDG of workpiece 2 and (d) to (h) DEDAG of workpiece 8

of discharge erosion and material softening, therefore the open circuit voltage E and grinding depth a_p were the most critical parameters, which were set as variables. CDG and CWG experiments of binderless WC workpieces were also designed as the control group. The detailed processing parameters are shown in Table 4. Some grinding and discharge parameters were set as follows: impulse width $T_{on} = 4 \mu s$, impulse interval $T_{off} = 4 \mu s$, spindle speed $N = 3000 \text{ r/min}$, and feed rate $v_f = 10 \text{ mm/min}$. The final machined workpieces are shown in Fig. 3d.

During the machining process, the voltage and current signals were collected by an oscilloscope (DHO800, RIGOL) with a current probe (RP1001C, RIGOL). The grinding chips were collected, and the scanning electron microscope (SEM) (Quanta 450 FEG, FEI) was used to

observe their morphologies. The micro hardness tester (FM-110, Future Tech) was used to measure the hardness of ground workpieces, where a Vickers indenter with an indentation load of 1000gf was used. The nanoindentation instrument (TI-950, Hysitron) was utilized to measure the residual stress of ground workpieces with Wang et al.'s model [36]. The Berkovich indenter with an indentation load of 50 mN was used. Five different positions were selected randomly for each measured workpiece, the values of hardness and residual stress for which were averaged. The SEM (Sigma300, ZEISS) was used to observe surface morphology. The non-contact laser profilometer (NH-3SPs, Mitaka Kohki Co.) was utilized to measure surface roughness R_a . The values of R_a for ten positions randomly selected from each workpiece were averaged.

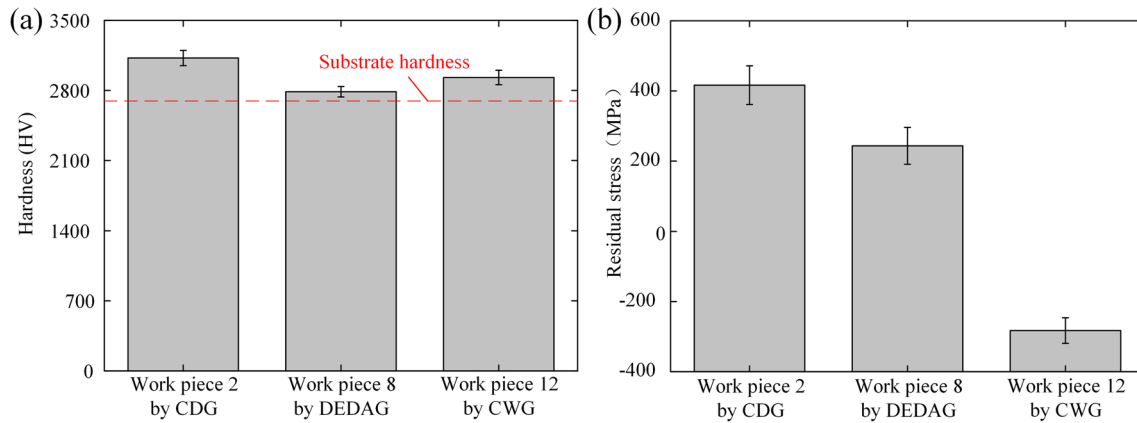


Fig. 6 **a** Hardness and **b** residual stress for workpieces 2 (ground by CDG), 8 (ground by DEDAG), and 12 (ground by CWG)

To observe the microscale subsurface morphology, the focused ion beam (FIB) (Helios600i, FEI) was first utilized to mill a pit ($40\ \mu\text{m} \times 20\ \mu\text{m} \times 20\ \mu\text{m}$) in workpieces 2, 8 and 12, and then the SEM (Sigma300, ZEISS) was used for observation. The FIB parameters were set as follows: the acceleration voltage was 30 keV; the ion beam current was set as 0.79 nA and 0.23 nA for rough and fine milling, respectively. To observe the nanoscale subsurface morphology, the same FIB was first used to cut a slice ($5\ \mu\text{m} \times 5\ \mu\text{m} \times 120$ to $150\ \text{nm}$) from workpieces 2, 8, and 12, and then the transmission electron microscope (TEM) (JEM-3200FS, JEOL) was utilized for observation. The FIB parameters were set as follows: the acceleration voltage and ion beam current were respectively set as 30 keV and 80 pA for thinning, and they were respectively set as 2 keV and 23 pA for polishing.

4 Results and Discussions

4.1 Electrical Properties During DEDAG Process

Figure 4 shows the current (I) and voltage (E) waveforms during the DEDAG process of binderless WC workpieces. Depending on the discharge gap, there are basically five states for a single pulse discharge waveform:

- (1) Open circuit (τ_0): the no-load state. The voltage value is equal to the pulse voltage provided by the pulse power supply.
- (2) Spark discharge (τ_d): the effective state. High-frequency clutter components and breakdown delay phenomena appear on the voltage waveform. At this time, the energy of the spark discharge plasma channel is highly concentrated and produces a sharp shock.
- (3) Transient arc discharge (τ_a): the transitional state. From the voltage pattern, the channel of transitional

discharge is easier to form than the channel of spark discharge. It can be restored to spark discharge by servo control or by changing the gap state.

- (4) Arc discharge: a harmful discharge state. It is not only easy to burn the workpiece but also has low material etching. Since no violent thermal explosion is formed during arc discharge, the surface material will only be melted and recast, rather than vaporized and removed.
- (5) Short circuit: the voltage is very low and the current waveform is smooth. There is no etching effect in a short circuit, making it is easy to form harmful phenomena such as arcing.

During the DEDAG process, the mechanism is different from traditional EDM due to the influence of the rotating tool electrode (the metal bond of the grinding wheel). On one hand, there is a rotary movement between the workpiece electrode and the tool electrode, causing the discharge point to continuously change with the relative rotation of the workpiece and the tool. On the other hand, the breakdown strength of air is less than that of the dielectric fluid, resulting in a smaller discharge gap. The chips, electro-etching residue, and other debris can be quickly removed from the gap, as well as the heat generated by the discharge. It also greatly reduces the possibility of arc discharge, thus ensuring the quality of processing.

4.2 Chip Morphology, Surface Hardness and Residual Stress

Figure 5a to c show the strip, shear, and flow chips generated during CDG of workpiece 2, respectively, and Fig. 5d to h show the strip, shear, flow, round, and broken chips produced during DEDAG of workpiece 8, respectively. Obviously, the chips during DEDAG have smaller size than those during CDG. Due to the discharge erosion,

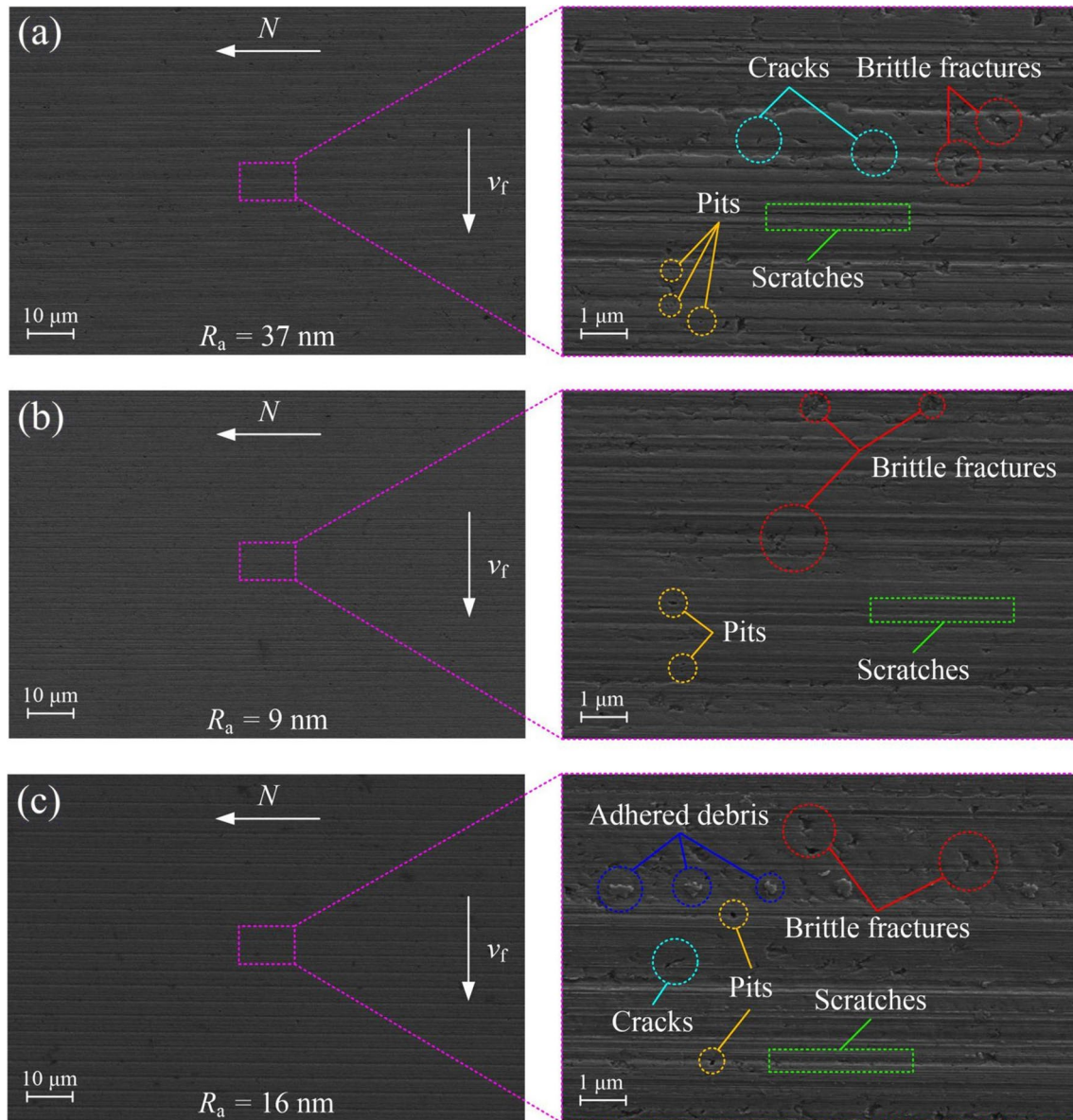


Fig. 7 SEM images of surface morphologies for workpieces (a) 2 (ground by CDG), (b) 8 (ground by DEDAG), and (c) 12 (ground by CWG)

some chips become round after melting, and some chips are broken during DEDAG, as shown in Fig. 5g and h, respectively. Smaller chips help to reduce the chip adhesion and maintain the enough space for holding chips, thereby reducing the effect of chip scratching on the ground surface, and improving the ground surface quality. Both strip and shear chips are formed by microcutting of abrasive grits, and abrasive grits with a negative rake angle (average value of 60 degrees) play an important role in microcutting workpieces. In the microcutting of the workpiece, the chip formation mechanism of the shear chip to a great extent is associated with the fracture of WC particles and the material slipping along the shear plane. The flow

chip is basically straight, indicating that there is no large plastic deformation in the chip formation process [37]. Therefore, more cracks are generated during the chip formation process. Smaller flow chips in DEDAG also imply smaller brittle-plastic critical transition depths, demonstrating that electrical erosion can reduce brittle removal during the DEDAG process of binderless WC and improve the ground surface quality.

Figure 6a and b show the hardness and residual stress for workpieces 2 (ground by CDG), 8 (ground by DEDAG), and 12 (ground by CWG), respectively. It can be found that the hardness by DEDAG is smaller than that by CDG or CWG, and the value of hardness by CDG is

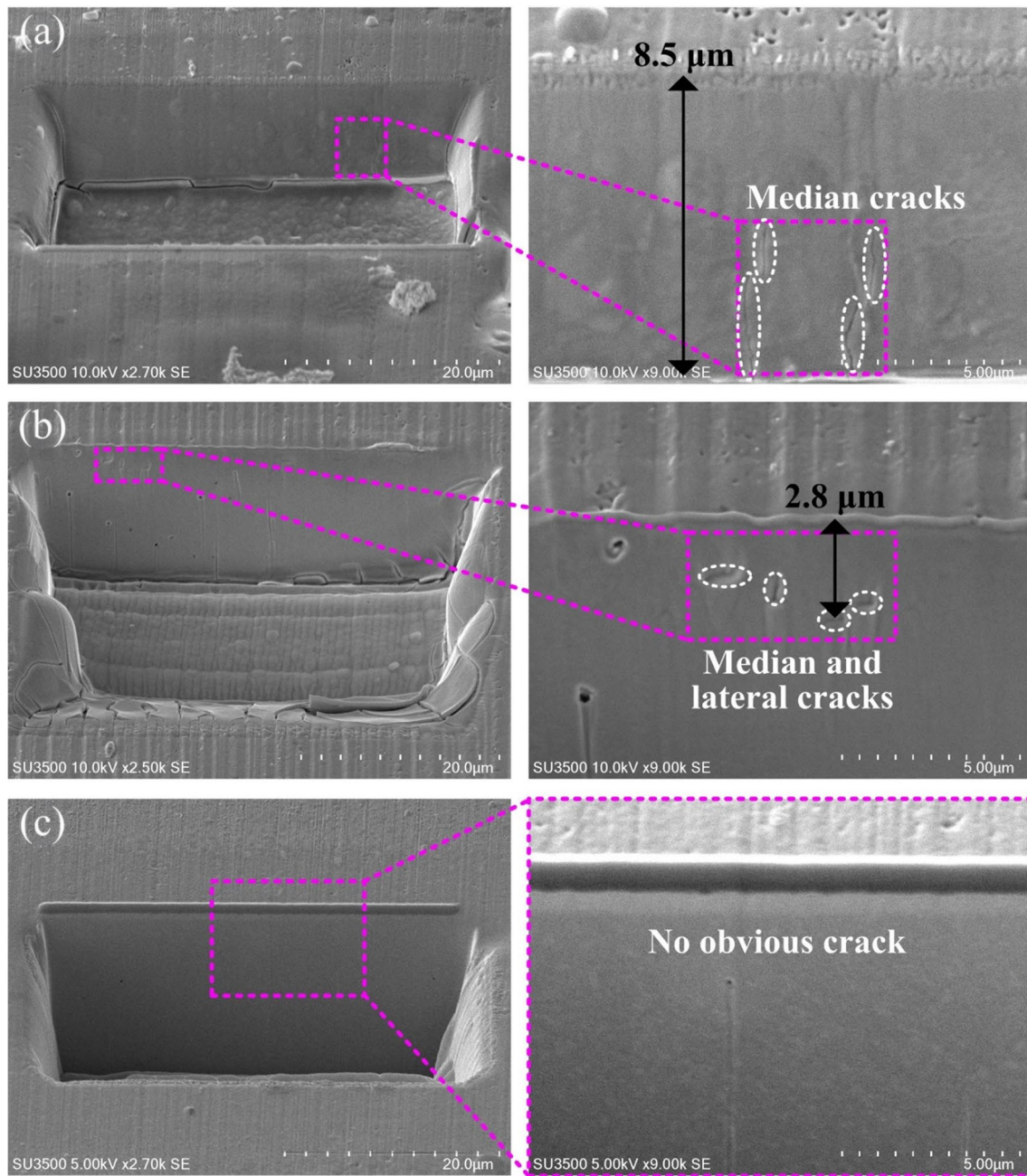


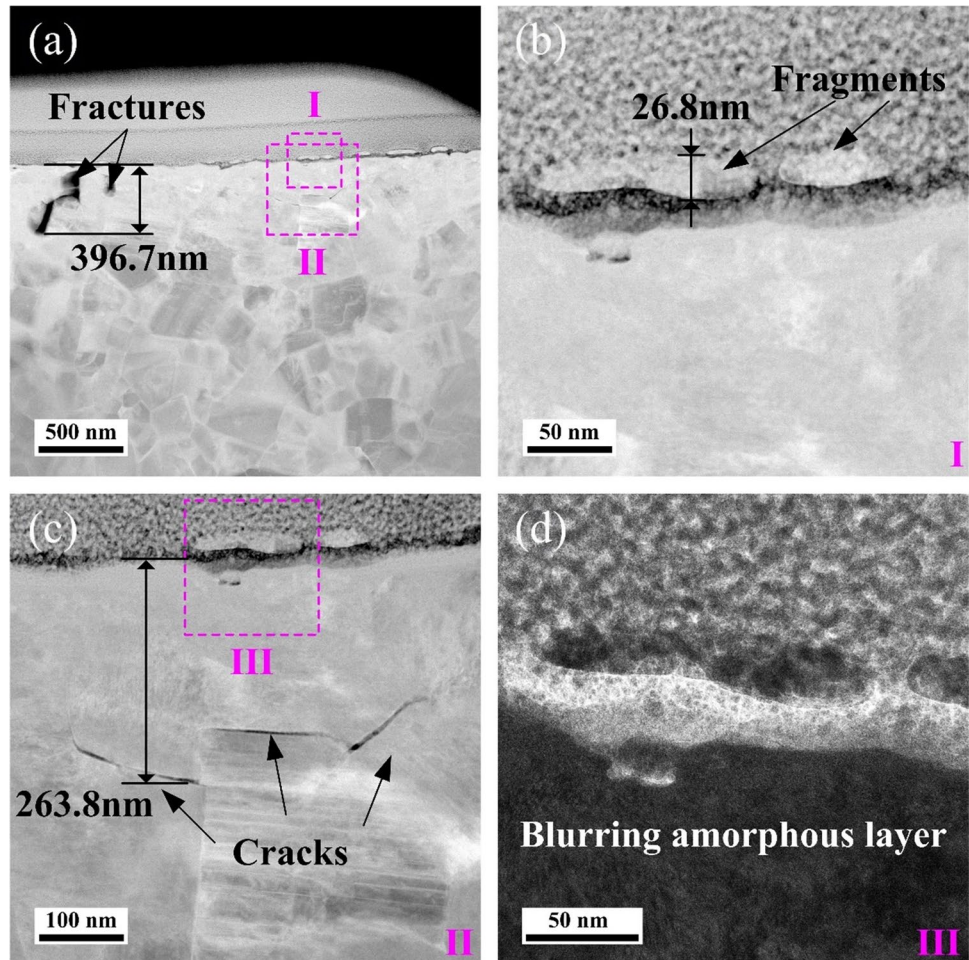
Fig. 8 Cross-section FIB/SEM images of microscale subsurface morphologies for workpieces (a) 2 (ground by CDG), (b) 8 (ground by DEDAG), and (c) 12 (ground by CWG)

12.1% larger than that by DEDAG, indicating that the discharge erosion can reduce the work hardening and soften the workpiece surface. In the grinding process, the factors influencing work hardening include machining extrusion caused by plastic deformation and microstructural changes in the surface layer caused by cutting heat. During the DEDAG process, the machined surface is subjected to less impact and extrusion by the abrasive grits. The lattice

distortion, grain deformation, and fragmentation occurring on the machined surface are minimal, which reduces the work hardening on the ground surface.

It can be found that the residual stress by CDG or DEDAG is tensile, while that by CWG is compressive, and the value of residual stress by CDG is about 1.7 times than that by DEDAG. The residual stress is generated due to the thermal and mechanical coupling effects during the grinding.

Fig. 9 a TEM image of nanoscale subsurface morphologies for workpiece 2 (ground by CDG). Partially enlarged views for (b) region (I) from (a), (c) region (II) from (a), and (d) region (III) from (c)



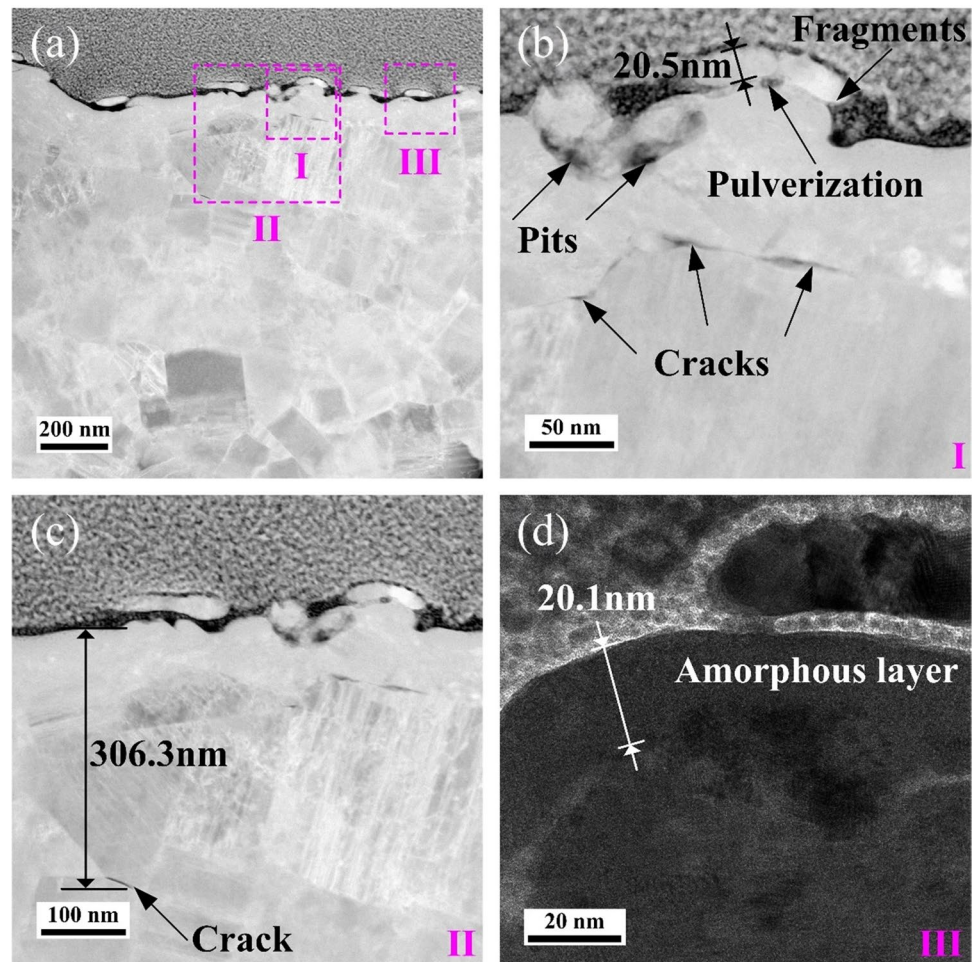
Generally, the residual compressive stress is induced by mechanical loads, while the residual tensile stress is caused by thermal loads [38]. Since thermal loads play a dominant role in the dry grinding [39], the residual tensile stress is found during CDG or DEDAG. During DEDAG, although many craters and recast layers with a high tensile stress may be produced by discharge erosion [40], they can be removed by abrasive scratching, resulting in a smaller tensile stress compared to that by CDG. During CWG, since grinding coolant changes heat distribution, the residual compressive stress is generated. Overall, DEDAG can soften/melt workpiece material and shrink grinding chips. Meanwhile, since residual tensile stress can reduce the fatigue strength of components, DEDAG has obvious advantage over CDG in residual stress.

4.3 Ground Surface Morphology

Figure 7a to c show the SEM images of surface morphologies for workpieces 2 (ground by CDG), 8 (ground by DEDAG), and 12 (ground by CWG), respectively. It can be

seen from Fig. 7a and c that there are many brittle fractures, cracks, pits, and scratches on the ground surface, indicating a brittle removal. The scratches shown in Fig. 7a are deeper than those shown in Fig. 7c, resulting in the surface roughness for the former ($R_a = 37$ nm) being larger than that for the latter ($R_a = 16$ nm). Only abrasive scratching is involved in CDG while scratching-erosion combination is involved in DEDAG, leading to that the brittle removal in CDG is more severe than that in DEDAG. In CWG, some adhered debris easily remains on the machined surface, as shown in Fig. 7c. This may be because as more and more grinding chips are accumulated and the chip holding space is decreased, part of chips may be squeezed on the ground surface by grinding wheel. Compared with Fig. 7a and c, Fig. 7b shows the best-machined surface quality with the smallest fractures/pits and the shallowest scratches, corresponding to a surface roughness of $R_a = 9$ nm. This indicates that the brittle fractures/pits and scratches can be reduced due to the unique material removal mechanism of DEDAG, i.e., discharge erosion and abrasive scratching. During the machining process of DEDAG, electrical erosion softens the surface material,

Fig. 10 a TEM image of nanoscale subsurface morphologies for workpiece 8 (ground by DEDAG). Partially enlarged views for (b) region (I) from (a), (c) region (II) from (a), and (d) region (III) from (a)



reduces the brittle-plastic critical transition depth and the material brittle removal. Thus, DEDAG can reduce damages such as pits and cracks, and improve the quality of the ground surface.

Although EDG and EDDG have been reported, there are few cases in which it is applied to binderless WC or WC/Co. Koshy et al. [16] studied EDDG on cemented carbide (WC-TiC-TaNb-C-Co), but the processing parameters were not optimized and the subsurface damage was not further studied. Singh et al. [17] used the EDDFG to process WC/Co (10wt.% Co) and obtained a machined surface with an average surface roughness (ASR) of 3.07 μm . Under similar grinding parameters, Kim et al. [14] used ELID grinding to process WC/Co, and obtained machined surfaces with surface roughness of R_a of 20 nm. In contrast, the surface roughness of the workpiece processed by DEDAG was 55% lower than that of ELID grinding.

In recent years, some other grinding methods had been proposed for processing binderless WC. For example, Guo et al. [12] used the novel ultrasonic vibration assisted grinding (UVAG) to process binderless WC with a 400# grinding wheel, and obtained the machined surface with R_a of 56 nm.

Yu et al. [41] used the CuSnFeNi/diamond composite and achieved the grinding of WC with $R_a = 14.92 \pm 2.92$ nm with a diamond abrasive size of 16 μm . The surface roughness R_a obtained by DEDAG is 48.9% higher than that by UVAG with the same diamond abrasive size, while it is close to that with the fine diamond grits. Overall, compared with other grinding methods of binderless WC or WC/Co cemented carbide, DEDAG has the advantage of high machined surface quality from the perspective of surface roughness.

4.4 Ground Subsurface Morphology

Figure 8a to c show the representative cross-section FIB/SEM images of microscale subsurface morphologies for workpieces 2 (ground by CDG), 8 (ground by DEDAG), and 12 (ground by CWG), respectively. Each cross-section is perpendicular to the scratch groove direction. It can be observed from Fig. 8a that there are many discontinuous median cracks generated in the subsurface. The maximum crack depth is 8.5 μm , which is slightly smaller than the grinding depth of 10 μm , and the crack length is about 2.5 μm . It can be found from Fig. 8b that there are many scattered subsurface median

Fig. 11 a TEM image of nanoscale subsurface morphologies for workpiece 12 (ground by CWG). Partially enlarged views for (b) region (I) from (a), (c) region (II) from (a), and (d) region (III) from (c)

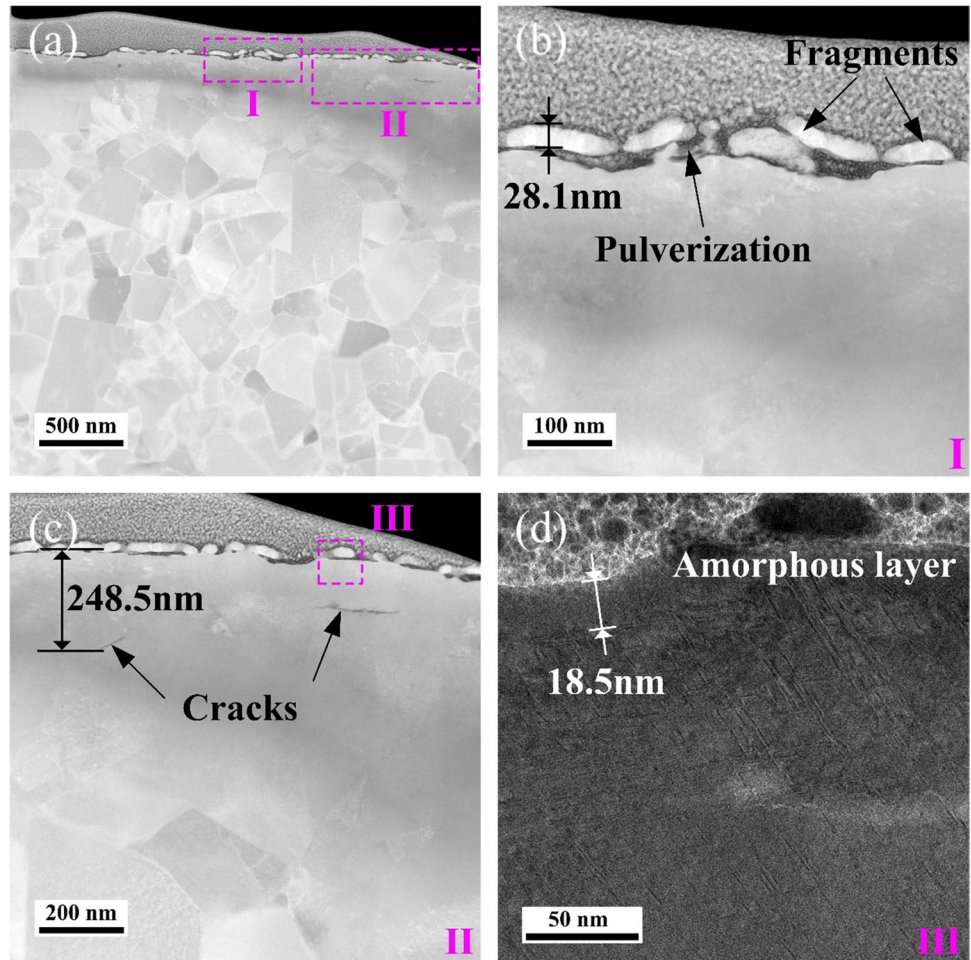


Fig. 12 SEM images of surface morphologies for workpieces (a) 3 ($E=20$ V), (b) 4 ($E=30$ V), (c) 5 ($E=40$ V), and (d) 6 ($E=50$ V) ground by DEDAG

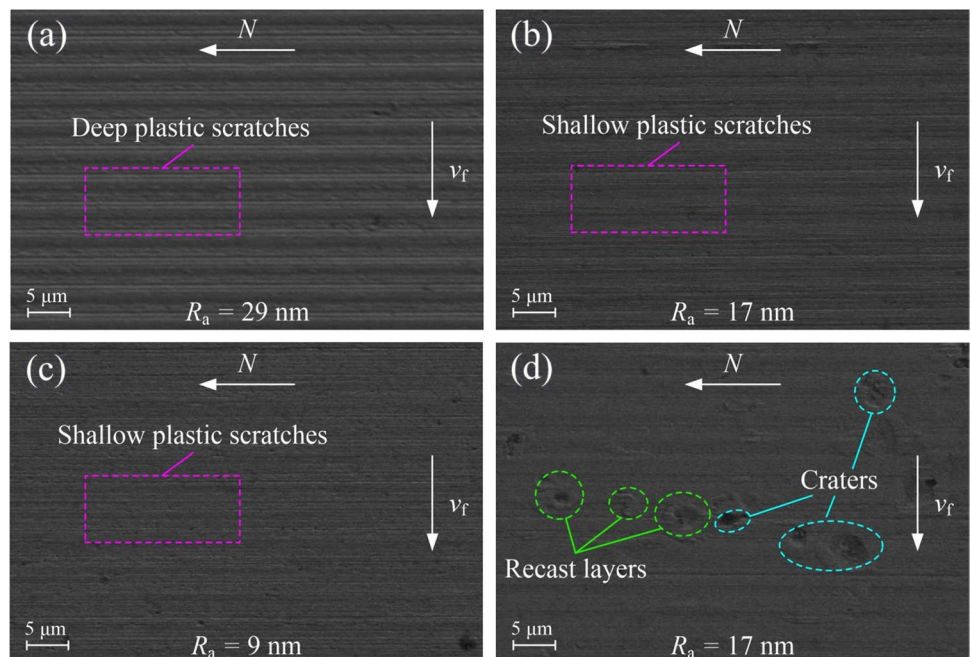
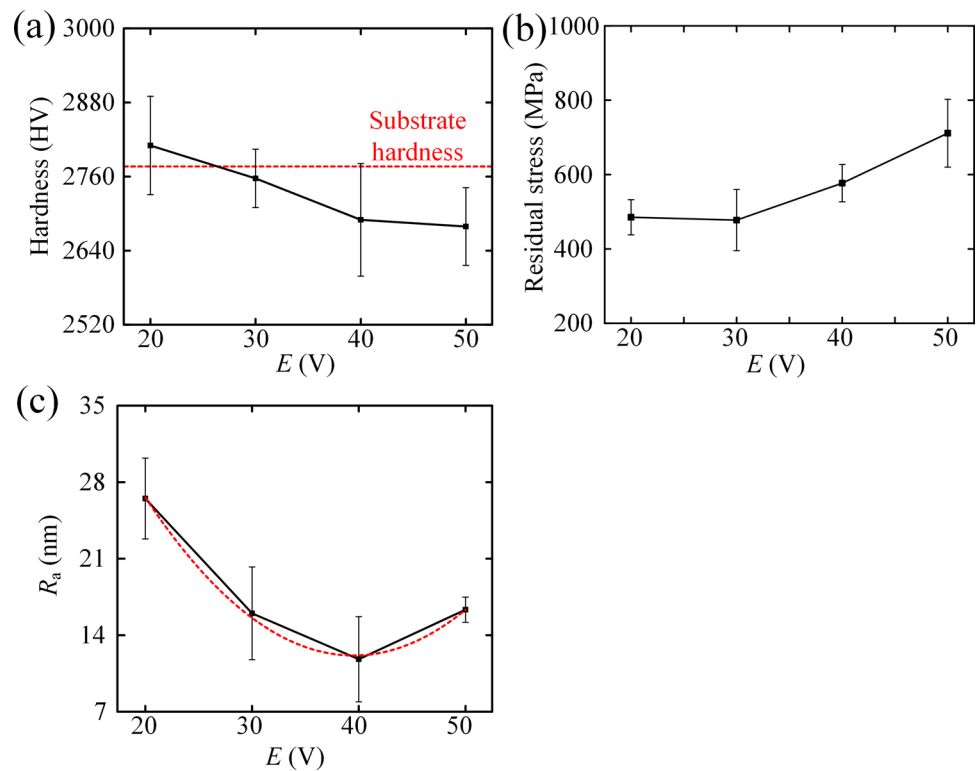


Fig. 13 Changing trend of (a) hardness, (b) residual stress, and (c) surface roughness R_a with open-circuit voltage E



and lateral cracks. The maximum crack depth is 2.8 μm , which is much smaller than the grinding depth of 10 μm , and the crack length is less than 1 μm . Both the crack depth and length induced by CDG are larger than those induced by DEDAG. Considering the crack sizes and the grain size (~ 600 nm) of binderless WC used, the crack propagation may be transgranular [42]. According to the indentation fracture mechanics of brittle materials, the median crack is usually nucleated beneath the plastic zone, and the lateral crack is usually initiated near the base of the plastic zone [43–45]. The plastic zone is generated due to the contact between the abrasive grit and the workpiece. It can be seen from Fig. 8c that there is no obvious subsurface crack. This indicates that DEDAG can lead to a larger SSD depth compared to CWG, while it can alleviate SSDs compared to CDG. Since the grinding coolant introduces environmental pollution, DEDAG has a certain advantage over CWG.

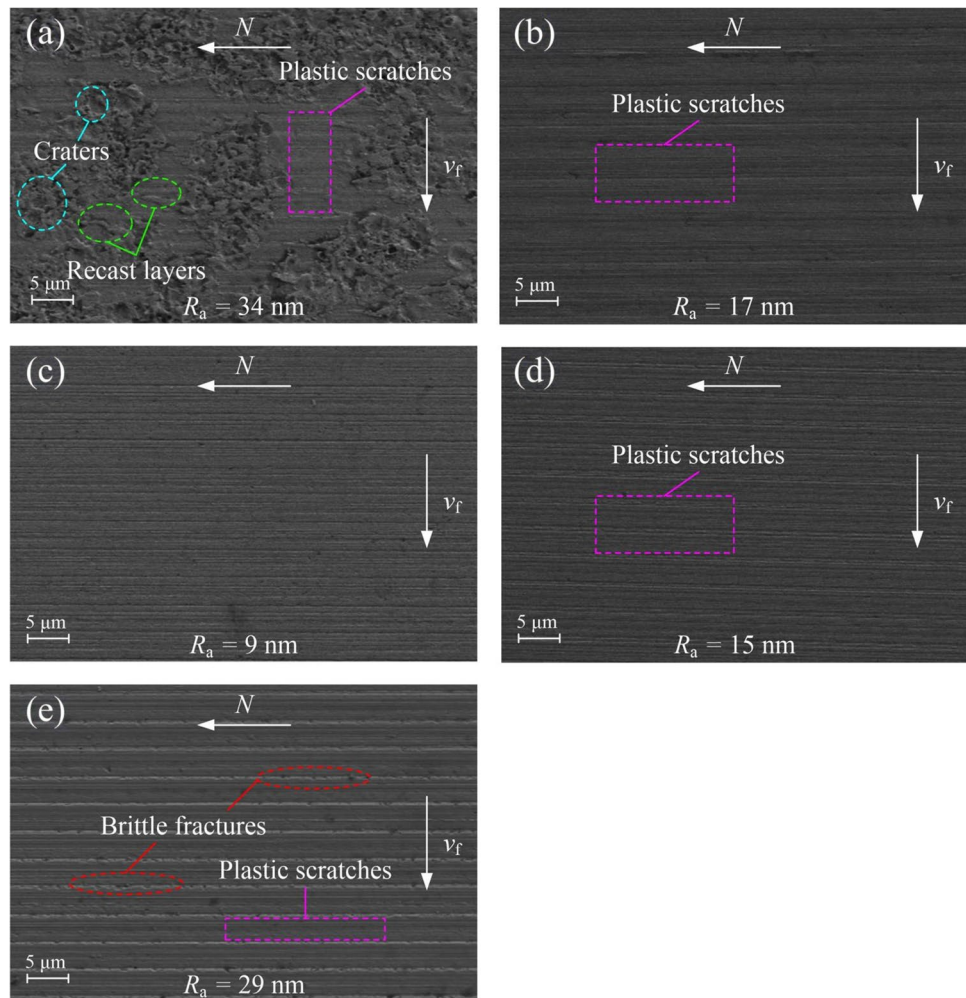
Figures 9a to d, 10a to d, and 11a to d show the representative TEM images of nanoscale subsurface morphologies for workpieces 2 (ground by CDG), 8 (ground by DEDAG), and 12 (ground by CWG), respectively. Figures 9a, 10a, or 11a indicate different grain sizes in binderless WC with an average grain size of 600 nm. It can be found from Fig. 9a to d that there are obvious surface fragments, subsurface fractures and cracks, and blurring amorphous layers on the near-surface. The fragments are generated due to the spalling of workpiece material with a thickness of ~ 26.8 nm. The depth of the deepest fracture and crack are about 396.7 nm and 263.8 nm, respectively. Due to the

high grinding force and temperature generated during the CDG process, the crystalline structure of binderless WC is disrupted seriously, leaving a dimly defined amorphous layer. There may be many dense crystal defects on the near-surface due to the severe grain deformation and stress release. The formation mechanism of the amorphous layer in a ground component can be interpreted as follows: The abrasion of the cutting edge of abrasive grits results in an amorphous phase transformation, while the high-speed impact between the abrasive grits and the workpiece enhances the penetration of oxygen [46]. As shown in Fig. 10a to d, there are many surface fragments, pits, pulverization, subsurface cracks, and uniformly distributed amorphous layers. The thicknesses of the fragment and amorphous layer are about 20.5 nm and 20.1 nm, respectively, and the maximum depth of subsurface crack is about 306.3 nm. It can be seen from Fig. 11a to d that the surface and subsurface characteristics are almost the same as those in Fig. 10a to d, with a fragment thickness of ~ 28.1 nm, the maximum crack depth of ~ 248.5 nm, and an amorphous layer thicknesses of ~ 18.5 nm. The above analysis indicates that the workpiece by DEDAG possesses a higher subsurface quality than that by CDG, while it has a similar one to that by CWG.

4.5 Effects of DEDAG Parameters on Ground Surface Quality

After verifying that DEDAG is an effective method of processing the binderless WC from the perspective of chip

Fig. 14 SEM images of surface morphologies for workpieces (a) 7 ($a_p = 1 \mu\text{m}$), (b) 3 ($a_p = 5 \mu\text{m}$), (c) 8 ($a_p = 10 \mu\text{m}$), (d) 9 ($a_p = 15 \mu\text{m}$), (e) 10 ($a_p = 20 \mu\text{m}$) ground by DEDAG

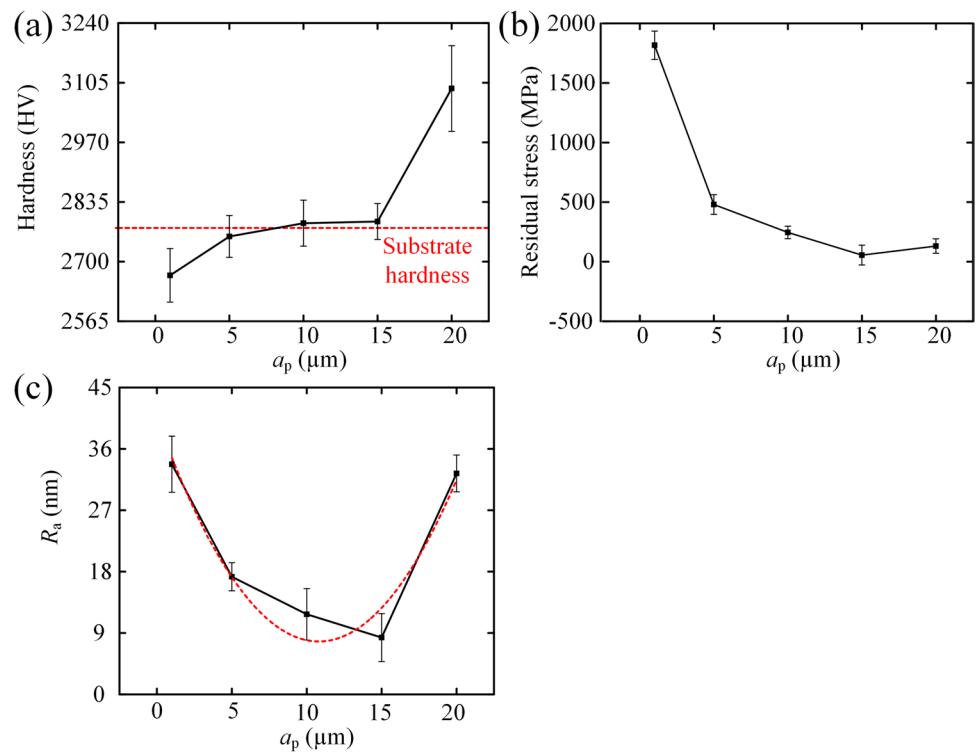


morphology, workpiece hardness, residual stress, surface roughness, and SSDs, the effects of DEDAG parameters (open-circuit voltage E , grinding depth a_p) on the machined surface are investigated experimentally. Figure 12a to d show the SEM images of surface morphologies for workpieces 3 ($E = 20 \text{ V}$), 4 ($E = 30 \text{ V}$), 5 ($E = 40 \text{ V}$), and 6 ($E = 50 \text{ V}$), respectively. As the circuit voltage E increases from 20 to 50 V, the surface quality becomes first better and then worse. When $E = 20 \text{ V}$, there are many deep plastic scratches on the ground surface. At this time, the workpiece material may be softened slightly by discharge erosion and then it is scratched by abrasive grits. When $E = 30 \text{ V}$ or 40 V , there are many shallow plastic scratches but almost no fracture on the ground surface. At this time, the softened layer becomes deep, and many craters may be generated while being removed by abrasive scratching. When E increases to 50 V , there are many large craters and recast layers on the ground surface, which cannot be removed by abrasive scratching. The recast layers are formed due to the rapid cooling and solidification of the molten material, which seem like built-up adhesion. It is not difficult to predict that

the number of craters and recast layers would increase and the surface quality would get worse with the increase of E . Figure 13a to c show the changing trend of hardness, residual stress, and surface roughness R_a with open-circuit voltage E (20 to 50 V). It can be found from Fig. 13a and b that with an increasing E , the hardness decreases gradually, while the residual stress decreases slightly at first and then increases gradually. When $E = 20 \text{ V}$, the softened layer depth is shallow and the abrasive scratching dominates the material removal, which leads to a very high hardness and a little high residual tensile stress due to the hardening effect. With an increasing E , the discharge erosion dominates the material removal gradually, and the softening effect, craters, and recast layers become more obvious, thereby decreasing the hardness while increasing the residual tensile stress. It can be seen from Fig. 13c that the lowest value of $R_a = 8 \text{ nm}$ corresponds to the optimum value of $E = 40 \text{ V}$ for DEDAG of binderless WC.

Figure 14a to e show the SEM images of surface morphologies for workpieces 7 ($a_p = 1 \mu\text{m}$), 3 ($a_p = 5 \mu\text{m}$), 8 ($a_p = 10 \mu\text{m}$), 9 ($a_p = 15 \mu\text{m}$), and 10 ($a_p = 20 \mu\text{m}$),

Fig. 15 Changing trend of (a) hardness, (b) residual stress, and (c) surface roughness R_a with grinding depth a_p



respectively. It can be found that as the grinding depth a_p increases from 1 μm to 20 μm , the machined surface quality becomes first better and then worse. When $a_p = 1 \mu\text{m}$, there are many craters, recast layers, and plastic zones on the ground surface when the material is mainly removed by discharge erosion. Currently, most abrasive grits do not contact the workpiece surface, and the material is removed by discharge erosion. The final workpiece surface profile is formed by craters. With the increase of a_p , most abrasive grits participate in the material removal, and the craters are gradually removed by abrasive scratching. Currently, the material is removed by scratching-erosion combination. When the craters are completely removed by abrasive scratching, the machined quality is considered the best. With the further increase of a_p , the abrasive grits will remove the material below the craters directly, and the machined quality is very poor. Figure 15a to c show the changing trend of hardness, residual stress, and surface roughness R_a with grinding depth a_p (1 to 20 μm). It can be found from Fig. 15a and b that when $a_p = 1 \mu\text{m}$, the hardness is smallest and the residual stress is largest due to the softening effect and the generation of craters and recast layers; With the increase of a_p , the hardness changes slightly while the residual stress decreases gradually due to the removal of craters; When $a_p = 20 \mu\text{m}$, the hardness increases suddenly and the residual stress increases slightly due to the dominant role of abrasive scratching. Figure 15c shows that the best value of R_a can reach up to 9 nm. Therefore,

for DEDAG of binderless WC, the optimal value of a_p ranges from 10 μm to 15 μm . It is worth noting that when $a_p = 1 \mu\text{m}$, electrical erosion dominates the material removal and the surface morphology is similar to that of conventional EDM, with some typical defects such as craters and cracks appearing in the HAZ [26].

5 Conclusions

Targeting on high quality and efficiency grinding of binderless tungsten carbide (WC), a clean and eco-friendly dry electrical discharge assisted grinding (DEDAG) method is proposed in this paper. The principle of DEDAG is revealed and the platform of DEDAG is developed. The current and voltage waveforms during the DEDAG process were observed, and the discharge properties were analyzed. By comparing the chip morphologies, workpiece hardness, residual stress, surface morphologies, and subsurface morphologies by CDG, DEDAG, and CWG, the effectiveness of DEDAG method is verified. By investigating the effects of DEDAG parameters on the machined surface quality, the optimal DEDAG parameters are determined. The main findings include:

- (1) Due to the unique material removal mechanism, i.e., diamond abrasive scratching, electrical discharge erosion, and scratching-erosion combination,

DEDAG can soften/melt the workpiece material, thereby promoting the plastic removal and suppressing the generation of SSDs. DEDAG can also shrink the grinding chips and realize the sharpening of grinding wheel.

- (2) Lower residual tensile stress is generated during DEDAG of binderless WC compared with CDG. In terms of surface roughness R_a , the surface quality of binderless WC by DEDAG is better than that by CDG or CWG. In terms of SSDs, the crystal structure deteriorates, and a fuzzy amorphous layer is left in binderless WC by CDG. In contrast, binderless WC by DEDAG has better crystal integrity, and its sub-surface quality is close to that by CWG.
- (3) The workpiece surface quality greatly depends on open-circuit voltage and grinding depth. With the increase of open-circuit voltage or grinding depth, the ground surface quality is first better and then worse. The optimal open-circuit voltage is 40 V and the optimal grinding depth ranges from 10 μm to 15 μm .

In the future, more processing parameters, such as spindle speed, feed rate, impulse width, and impulse interval will be considered for optimizing the DEDAG of binderless WC. More characterization, such as elemental composition/proportion generated on the machined surface, will be conducted for revealing the DEDAG mechanism of binderless WC.

Acknowledgements The authors would like to express thanks to the National Natural Science Foundation of China (51805334), the Natural Science Foundation of Guangdong Province (2023A1515030249), the Innovation and Technology Commission (ITC) of the Government of the Hong Kong Special Administrative Region, China (GHP/142/19SZ) and the Research and Innovation Office of The Hong Kong Polytechnic University (BBR8).

Funding Open access funding provided by The Hong Kong Polytechnic University.

Data Availability Data are included within this article. Additional data related to this study will be available upon reasonable request.

Declarations

Competing Interest The authors declare that they have no known competing financial interests or personal relationships that could have appeared to influence the work reported in this paper.

Open Access This article is licensed under a Creative Commons Attribution 4.0 International License, which permits use, sharing, adaptation, distribution and reproduction in any medium or format, as long as you give appropriate credit to the original author(s) and the source, provide a link to the Creative Commons licence, and indicate if changes were made. The images or other third party material in this article are included in the article's Creative Commons licence, unless indicated otherwise in a credit line to the material. If material is not included in the article's Creative Commons licence and your intended use is not

permitted by statutory regulation or exceeds the permitted use, you will need to obtain permission directly from the copyright holder. To view a copy of this licence, visit <http://creativecommons.org/licenses/by/4.0/>.

References

1. Poetschke, J., Richter, V., & Holke, R. (2012). Influence and effectivity of VC and Cr_3C_2 grain growth inhibitors on sintering of binderless tungsten carbide. *International Journal of Refractory Metals and Hard Materials*, 31, 218–223. <https://doi.org/10.1016/j.ijrmhm.2011.11.006>
2. Wu, M., Guo, B., Zhao, Q., & He, P. (2018). Precision grinding of a microstructured surface on hard and brittle materials by a microstructured coarse-grained diamond grinding wheel. *Ceramics International*, 44(7), 8026–8034. <https://doi.org/10.1016/j.ceramint.2018.01.243>
3. Zhang, Q., Guo, N., Chen, Y., & To, S. (2019). Effects of binder concentration on the nanometric surface characteristics of WC-Co materials in ultra-precision grinding. *International Journal of Refractory Metals and Hard Materials*, 85(2019), 105048. <https://doi.org/10.1016/j.ijrmhm.2019.105048>
4. Sun, J., Zhao, J., Huang, Z., Yan, K., Shen, X., Xing, J., Gao, Y., Jian, Y., Yang, H., & Li, B. (2020). A review on binderless tungsten carbide: Development and application. *Nano-Micro Letters*, 12, 1–37. <https://doi.org/10.1007/s40820-019-0346-1>
5. Carreira, L. A. S., Hassui, A., & Ventura, C. E. H. (2023). Energy efficiency assessment in plunge-face grinding of cemented tungsten carbide cutting inserts. *International Journal of Precision Engineering and Manufacturing-Green Technology*. <https://doi.org/10.1007/s40684-023-00518-3>
6. Micallef, C., Zhuk, Y., & Aria, A. I. (2020). Recent progress in precision machining and surface finishing of tungsten carbide hard composite coatings. *Coatings*, 10, 731. <https://doi.org/10.3390/coatings10080731>
7. Bulla, B., Klocke, F., & Dambon, O. (2012). Analysis on ductile mode processing of binderless, nano crystalline tungsten carbide through ultra precision diamond turning. *Journal of Materials Processing Technology*, 212(5), 1022–1029. <https://doi.org/10.1016/j.jmatprotec.2011.12.010>
8. You, K., & Fang, F. (2022). High effective laser assisted diamond turning of binderless tungsten carbide. *Journal of Materials Processing Technology*, 302(2022), 117505. <https://doi.org/10.1016/j.jmatprotec.2022.117505>
9. Meng, Q., Guo, B., Wu, G., Li, C., Xiang, Y., Guo, Z., Jia, J., & Zhao, Q. (2023). Accurate modeling and controlling of weak stiffness grinding system dynamics with microstructured tools. *Mechanical Systems and Signal Processing*, 201, 110659. <https://doi.org/10.1016/j.ymssp.2023.110659>
10. Zhang, Q., Zhao, Q., To, S., Guo, B., & Rao, Z. (2018). Precision machining of 'water-drop' surface by single point diamond grinding. *Precision Engineering*, 51, 190–197. <https://doi.org/10.1016/j.precisioneng.2017.08.010>
11. Guo, B., Zhao, Q., & Jackson, M. J. (2012). Precision grinding of binderless ultrafine tungsten carbide (WC) microstructured surfaces. *The International Journal of Advanced Manufacturing Technology*, 64(5–8), 727–735. <https://doi.org/10.1007/s00170-012-4068-5>
12. Guo, B., & Zhao, Q. (2017). Ultrasonic vibration assisted grinding of hard and brittle linear micro-structured surfaces. *Precision Engineering*, 48, 98–106. <https://doi.org/10.1016/j.precisioneng.2016.11.009>
13. Yan, G., You, K., & Fang, F. (2019). Three-linear-axis grinding of small aperture aspheric surfaces. *International Journal of*

- Precision Engineering and Manufacturing-Green Technology*, 7(5), 997–1008. <https://doi.org/10.1007/s40684-019-00103-7>
14. Kim, J. D., & Lee, F. S. (1999). A study of the mirror-like grinding of sintered carbide with optimum in-process electrolytic dressing. *International Journal of Advanced Manufacturing Technology*, 15(9), 615–623. <https://doi.org/10.1007/s001700050110>
 15. Stephenson, D. J., Hedge, J., & Corbett, J. (2002). Surface finishing of Ni-Cr-B-Si composite coatings by precision grinding. *International Journal of Machine Tools & Manufacture*, 42(3), 357–363. [https://doi.org/10.1016/s0890-6955\(01\)00127-4](https://doi.org/10.1016/s0890-6955(01)00127-4)
 16. Koshy, P., Jain, V. K., & Lal, G. K. (1997). Grinding of cemented carbide with electrical spark assistance. *Journal of Materials Processing Technology*, 72(1), 61–68. [https://doi.org/10.1016/s0924-0136\(97\)00130-1](https://doi.org/10.1016/s0924-0136(97)00130-1)
 17. Singh, G. K., Yadava, V., & Kumar, R. (2010). Diamond face grinding of WC-Co composite with spark assistance: Experimental study and parameter optimization. *International Journal of Precision Engineering and Manufacturing*, 11(4), 509–518. <https://doi.org/10.1007/s12541-010-0059-3>
 18. Yadav, S. K. S., & Yadava, V. (2013). Experimental investigations to study electrical discharge diamond cutoff grinding (EDDCG) machinability of cemented carbide. *Materials and Manufacturing Processes*, 28(10), 1077–1081. <https://doi.org/10.1080/10426914.2013.792414>
 19. Neto, O. M. P., Calleja-Ochoa, A., Ayesta, I., Rodríguez, A., González-Barrio, H., & de Lacalle, L. N. L. (2024). A cleaner milling process replacing emulsion coolant by cryogenics CO₂. *International Journal of Precision Engineering and Manufacturing-Green Technology*, 11(1), 21–32. <https://doi.org/10.1007/s40684-023-00530-7>
 20. Huang, X., Zhang, J., Peng, K., Na, Y., Xiong, Y., Liu, W., Liu, J., Lu, L., & Li, S. (2019). Functional magnetic nanoparticles for enhancing ultrafiltration of waste cutting emulsions by significantly increasing flux and reducing membrane fouling. *Journal of Membrane Science*, 573, 73–84. <https://doi.org/10.1016/j.memsci.2018.11.074>
 21. Dai, Y. T., Ohmori, H., Watanabe, Y., Eto, H., Lin, W. M., & Suzuki, T. (2004). Subsurface properties of ceramics for lightweight mirrors after ELID grinding. *Jsm International Journal Series C-Mechanical Systems Machine Elements and Manufacturing*, 47(1), 66–71. <https://doi.org/10.1299/jsmec.47.66>
 22. Lu, Y. J., Sun, J. J., Wu, X. Y., & Chen, F. M. (2023). On-line prediction of impulse spark and arc discharge removals of metal bond in dry electrical discharge dressing of diamond grinding wheel. *International Journal of Precision Engineering and Manufacturing-Green Technology*, 10(2), 293–310. <https://doi.org/10.1007/s40684-022-00445-9>
 23. Wan, D. P., Wang, Y., & Hu, D. J. (2008). In situ truing/dressing of diamond wheel for precision grinding. *Chinese Journal of Mechanical Engineering*, 21(3), 46–51. <https://doi.org/10.3901/CJME.2008.03.046>
 24. Boopathi, S. (2022). An extensive review on sustainable developments of dry and near-dry electrical discharge machining processes. *Journal of Manufacturing Science and Engineering-Transactions of the ASME* 144 (5). <https://doi.org/10.1115/1.4052527>
 25. Yu, Z. B., Jun, T., & Masanori, K. (2004). Dry electrical discharge machining of cemented carbide. *Journal of Materials Processing Technology*, 149(1–3), 353–357. <https://doi.org/10.1016/j.jmatp.rotec.2003.10.044>
 26. Jahan, M. P., Rahman, M., & Wong, Y. S. (2011). A review on the conventional and micro-electrodischarge machining of tungsten carbide. *International Journal of Machine Tools and Manufacture*, 51(12), 837–858. <https://doi.org/10.1016/j.ijmactools.2011.08.016>
 27. Rao, X., Zhang, F., Lu, Y., Luo, X., & Chen, F. (2020). Surface and subsurface damage of reaction-bonded silicon carbide induced by electrical discharge diamond grinding. *International Journal of Machine Tools and Manufacture*, 154, 103564. <https://doi.org/10.1016/j.ijmactools.2020.103564>
 28. Zhou, T., Ma, F., Ruan, B., Zhou, J., Liew, P., & Wang, X. (2019). Microlens array fabrication on WC mold using EDM milling with in situ electrode trimming. *The International Journal of Advanced Manufacturing Technology*, 103(5–8), 3003–3011. <https://doi.org/10.1007/s00170-019-03731-0>
 29. Xie, J., & Tamaki, J. (2008). An experimental study on discharge mediums used for electro-contact discharge dressing of metal-bonded diamond grinding wheel. *Journal of Materials Processing Technology*, 208(1–3), 239–244. <https://doi.org/10.1016/j.jmatp.rotec.2007.12.115>
 30. Satyarathi, M. K., & Pandey, P. M. (2013). Modeling of material removal rate in electric discharge grinding process. *International Journal of Machine Tools and Manufacture*, 74, 65–73. <https://doi.org/10.1016/j.ijmactools.2013.07.008>
 31. Meng, Q., Guo, B., Zhao, Q., Li, H. N., Jackson, M. J., Linke, B. S., & Luo, X. (2023). Modelling of grinding mechanics: A review. *Chinese Journal of Aeronautics*, 36(7), 25–39. <https://doi.org/10.1016/j.cja.2022.10.006>
 32. Albinski, K., Musiol, K., Miernikiewicz, A., Labuz, S., & Malota, M. (1996). The temperature of a plasma used in electrical discharge machining. *Plasma Sources Science & Technology*, 5(4), 736–742. <https://doi.org/10.1088/0963-0252/5/4/015>
 33. Clijsters, S., Liu, K., Reynaerts, D., & Lauwers, B. (2010). EDM technology and strategy development for the manufacturing of complex parts in SiSiC. *Journal of Materials Processing Technology*, 210(4), 631–641. <https://doi.org/10.1016/j.jmatp.rotec.2009.11.012>
 34. Keitel, M., Denkena, B., & Bergmann, B. (2024). Dry grinding by means of additively manufactured toric grinding pins. *International Journal of Precision Engineering and Manufacturing-Green Technology*, 11(2), 381–390. <https://doi.org/10.1007/s40684-023-00548-x>
 35. Lu, Y. J., Xie, J., & Si, X. H. (2015). Study on micro-topographical removals of diamond grain and metal bond in dry electro-contact discharge dressing of coarse diamond grinding wheel. *International Journal of Machine Tools and Manufacture*, 88, 118–130. <https://doi.org/10.1016/j.ijmactools.2014.09.008>
 36. Wang, Q., Ozaki, K., Ishikawa, H., Nakano, S., & Ogiso, H. (2006). Indentation method to measure the residual stress induced by ion implantation. *Nuclear Instruments and Methods in Physics Research Section B: Beam Interactions with Materials and Atoms*, 242(1–2), 88–92. <https://doi.org/10.1016/j.nimb.2005.08.008>
 37. Du, J. G., Zhou, L., Li, J. G., & Yao, Y. X. (2014). Analysis of chip formation mechanism in mill-grinding of SiCp/Al composites. *Materials and Manufacturing Processes*, 29(11–12), 1353–1360. <https://doi.org/10.1080/10426914.2014.912309>
 38. Azarhoushang, B., Daneshi, A., & Lee, D. H. (2017). Evaluation of thermal damages and residual stresses in dry grinding by structured wheels. *Journal of Cleaner Production*, 142, 1922–1930. <https://doi.org/10.1016/j.jclepro.2016.11.091>
 39. Zhang, Z., Sui, M., Li, C., Zhou, Z., Liu, B., Chen, Y., Said, Z., Debnath, S., & Sharma, S. (2022). Residual stress of grinding cemented carbide using MoS₂ nano-lubricant. *The International Journal of Advanced Manufacturing Technology*, 119(9–10), 5671–5685. <https://doi.org/10.1007/s00170-022-08660-z>
 40. Rahim, M. Z., Li, G., Ding, S., Mo, J., & Brandt, M. (2015). Electrical discharge grinding versus abrasive grinding in polycrystalline diamond machining—tool quality and performance analysis. *The International Journal of Advanced Manufacturing Technology*, 85(1–4), 263–277. <https://doi.org/10.1007/s00170-015-7935-z>
 41. Yu, J., Huang, L., Luo, H., & Hai, Y. (2019). Study effects on diamond concentration of CuSnFeNi/diamond composite on

grinding WC. *The International Journal of Advanced Manufacturing Technology*, 104(5–8), 2863–2873. <https://doi.org/10.1007/s00170-019-04033-1>

42. Li, C., Zhang, F., Wang, X., & Rao, X. (2018). Repeated nanoscratch and double nanoscratch tests of Lu_2O_3 transparent ceramics: Material removal and deformation mechanism, and theoretical model of penetration depth. *Journal of the European Ceramic Society*, 38(2), 705–718. <https://doi.org/10.1016/j.jeurceramsoc.2017.09.028>
43. Xiao, H., Zhang, F., Yin, S., Cheung, C. F., & Wang, C. (2023). Subsurface damage model in single and double scratching of fused silica with a blunt indenter. *International Journal of Mechanical Sciences*, 250, 108309. <https://doi.org/10.1016/j.ijmecsci.2023.108309>
44. Xiao, H., Wang, H., Yu, N., Liang, R., Tong, Z., Chen, Z., & Wang, J. (2019). Evaluation of fixed abrasive diamond wire sawing induced subsurface damage of solar silicon wafers. *Journal of Materials Processing Technology*, 273, 116267. <https://doi.org/10.1016/j.jmatprotec.2019.116267>
45. Xiao, H., Yin, S., Wang, H., Liu, Y., Wu, H., Liang, R., & Cao, H. (2021). Models of grinding-induced surface and subsurface damages in fused silica considering strain rate and micro shape/geometry of abrasive. *Ceramics International*, 47(17), 24924–24941. <https://doi.org/10.1016/j.ceramint.2021.05.220>
46. Zarudi, I., & Zhang, L. C. (1998). Effect of ultraprecision grinding on the microstructural change in silicon monocrystals. *Journal of Materials Processing Technology*, 84(1), 149–158. [https://doi.org/10.1016/S0924-0136\(98\)00090-9](https://doi.org/10.1016/S0924-0136(98)00090-9)

Publisher's Note Springer Nature remains neutral with regard to jurisdictional claims in published maps and institutional affiliations.



Yanjun Lu is an associate professor at Shenzhen University of China. He received his Ph.D degree from South China University of Technology in 2015. Now, he serves as the director of the Joint Training Postgraduate Demonstration Base of Guangdong Province, selected as Science and Technology Commissioner of Guangdong Province, 100 innovative doctoral & post-doctoral fellows in Guangdong Province, Shenzhen High-level talents, and senior members of Chinese Mechanical Engineering

Society. His research interests include dressing and truing of coarse diamond grinding wheel, micro-structure grinding, micro injection molding of LED light guide plate and biomedical microfluidic chip, etc.



Xingyu Mou is a master degree candidate in Mechanical Engineering at Shenzhen University of China. His main research is precision electrical discharge grinding.



Huapan Xiao is currently a postdoctoral at the State Key Laboratory of Ultra-precision Machining Technology, The Hong Kong Polytechnic University. He received his PHD degree in mechanical engineering from Xi'an Jiaotong University in 2020. His research interests include precision/ultra-precision machining and measuring technology.



Kangsen Li is a postdoctoral at The Hongkong Polytechnic University. He received his PHD degree in optical engineering from Shenzhen University in 2021. He is the author of more than 20 journal papers. His current research interests include precision manufacturing, optical lens, glass molding, optical imaging, and advanced material.



Chunjin Wang is a Research Assistant Professor at the State Key Laboratory of Ultra-precision Machining Technology, Department of Industrial and Systems Engineering, The Hong Kong Polytechnic University. His research interests are focused on polishing, ultra-precision machining technology, and functional structured surfaces.